A comparative study on fluorescent cholesterol analogs as versatile cellular reporters

Sezgin, Erdinc; Betul Can, Fatma ; Schneider, Falk; Clausen, Mathias P.; Galiani, Silvia; Stanly, Tess A.; Waithe, Dominic; Colaco, Alexandria ; Honigmann, Alf; Wüstner, Daniel; Platt, Frances; Eggeling, Christian

Published in:
Journal of Lipid Research

DOI:
10.1194/jlr.M065326

Publication date:
2016

Document version
Publisher's PDF, also known as Version of record

Citation for pulished version (APA):
Sezgin, E., Betul Can, F., Schneider, F., Clausen, M. P., Galiani, S., Stanly, T. A., ... Eggeling, C. (2016). A comparative study on fluorescent cholesterol analogs as versatile cellular reporters. Journal of Lipid Research, 57, 299-309. DOI: 10.1194/jlr.M065326

A comparative study on fluorescent cholesterol analogs as versatile cellular reporters[S]

Erdinc Sezgin,[1,*] Fatma Betul Can,[*] Falk Schneider,[*] Mathias P. Clausen,[*,†] Silvia Galiani,[*] Tess A. Stanly,[*] Dominic Waithe,[*] Alexandria Colaco,[§] Alf Honigmann,[**] Daniel Wüstner,[††] Frances Platt,[§] and Christian Eggeling[1,*]

MRC Human Immunology Unit,* Weatherall Institute of Molecular Medicine, University of Oxford, OX39DS Oxford, United Kingdom; MEMPHYS-Center for Biomembrane Physics, Department of Physics, Chemistry, and Pharmacy,† and Department of Biochemistry and Molecular Biology,†† University of Southern Denmark, 5230 Odense M, Denmark; Department of Pharmacology,§ University of Oxford, OX13QT Oxford, United Kingdom; and Max Planck Institute of Cell Biology and Genetics,** 01307 Dresden, Germany

Abstract Cholesterol (Chol) is a crucial component of cellular membranes, but knowledge of its intracellular dynamics is scarce. Thus, it is of utmost interest to develop tools for visualization of Chol organization and dynamics in cells and tissues. For this purpose, many studies make use of fluorescently labeled Chol analogs. Unfortunately, the introduction of the label may influence the characteristics of the analog, such as its localization, interaction, and trafficking in cells; hence, it is important to get knowledge of such bias. In this report, we compared different fluorescent lipid analogs for their performance in cellular assays: *1*) plasma membrane incorporation, specifically the preference for more ordered membrane environments in phase-separated giant unilamellar vesicles and giant plasma membrane vesicles; *2*) cellular trafficking, specifically subcellular localization in Niemann-Pick type C disease cells; and *3*) applicability in fluorescence correlation spectroscopy (FCS)-based and super-resolution stimulated emission depletion-FCS-based measurements of membrane diffusion dynamics. The analogs exhibited strong differences, with some indicating positive performance in the membrane-based experiments and others in the intracellular trafficking assay. However, none showed positive performance in all assays. Our results constitute a concise guide for the careful use of fluorescent Chol analogs in visualizing cellular Chol dynamics.—Sezgin, E., F. B. Can, F. Schneider, M. P. Clausen, S. Galiani, T. A. Stanly, D. Waithe, A. Colaco, A. Honigmann, D. Wüstner, F. Platt, and C. Eggeling. **A comparative study on fluorescent cholesterol analogs as versatile cellular reporters.** ***J. Lipid Res.*** **2016.** 57: **299–309.**

Supplementary key words cholesterol/trafficking • fluorescence microscopy • cholesterol/metabolism • lipid rafts • Niemann-Pick type C disease • membranes/model • giant unilamellar vesicles • giant plasma membrane vesicles • fluorescence correlation spectroscopy • stimulated emission depletion

Cholesterol (Chol) plays a pivotal role in eukaryotic cellular membranes both structurally and functionally (1, 2). Besides its specific involvement in cellular signaling (3–6), it also considerably shapes the architecture of the plasma membrane (7). Trafficking of Chol to the cell membrane is tightly regulated and plays an important role in cell metabolism (8). Hence, it is essential to visualize cellular Chol organization and to measure dynamics (such as uptake, diffusion, trafficking, and localization) with high specificity and sensitivity. In fluorescence microscopy, visualization of Chol can be achieved by using fluorescent Chol-binding molecules, such as filipin and specific fluorescently labeled peptides (9), intrinsically fluorescent mimics of Chol, such as cholestatrienol (CTL) and dehydroergosterol (DHE) (10, 11), or organic dye-labeled Chol analogs (12). Filipin and Chol-binding peptides have the potential to observe endogenous Chol, i.e., to be less artificial. Unfortunately, biasing by cross-linking of several

This work was supported by funding from the Wolfson Foundation, the Medical Research Council (MRC, Grants MC_UU_12010/unit programmes G0902418 and MC_UU_12025), MRC/BBSRC/ESPRC (Grant MR/K01577X/1), and the Wellcome Trust (Grant 104924/14/Z/14). E.S. was supported by EMBO Long Term and Marie Curie Intra-European Fellowships (MEMBRANE DYNAMICS). M.P.C. was supported by the Alfred Benzon Foundation research stipend. D.W. acknowledges support from the Villum and Novo Nordisk Foundation. A.C. and F.P. acknowledge the European Union Seventh Framework Programme (FP7 2007–2013, "Sphingonet", grant agreement 289278). F.P. is a Royal Society Wolfson Research Merit Award holder.

Manuscript received 16 November 2015 and in revised form 17 December 2015.

Published, JLR Papers in Press, December 21, 2015
DOI 10.1194/jlr.M065326

Abbreviations: Chol, cholesterol; *cpm*, counts per molecule; CTL, cholestatrienol; CW, continuous-wave; DChol, 6-dansyl-cholesterol; DHE, dehydroergosterol; DOPC, 1,2-dioleoyl-*sn*-glycero-3-phosphocholine; ERC, endocytic recycling compartment; FCS, fluorescence correlation spectroscopy; GPMV, giant plasma membrane vesicle; GUV, giant unilamellar vesicle; Ld, liquid disordered; Lo, liquid ordered; %Lo, liquid ordered partitioning coefficient; NBD, 7-nitrobenz-2-oxa-1,3-diazol-4-yl; NPC, Niemann-Pick type C; PCC, Pearson correlation coefficient; SLB, supported lipid bilayer; STED, stimulated emission depletion; TF, TopFluor; TF-Chol, TopFluor cholesterol.

[1] To whom correspondence should be addressed.
e-mail: erdinc.sezgin@rdm.ox.ac.uk (E.S.); christian.eggeling@rdm.ox.ac.uk (C.E.)

[S] The online version of this article (available at http://www.jlr.org) contains a supplement.

Chol molecules by the Chol-binding peptides cannot be excluded. Filipin involves the least disturbance on the native Chol molecule, but its specificity for Chol is questionable (13). In addition, proper labeling of cells with filipin requires their fixation, such that pulse-chase or time-lapse studies with living cells are not practicable. Also, filipin labels all cellular Chol pools equally, such that endogenous Chol made by the cell cannot be discriminated from lipoprotein-derived Chol or from Chol circulating specifically between the plasma membrane and intracellular organelles. For such investigations, fluorescent analogs of Chol are required. As has been shown before in various reports (10, 11, 14–21), natural Chol analogs such as DHE and CTL are, in principle, the most suitable molecules to mimic Chol. They can be inserted specifically into the plasma membrane or delivered to cells as part of lipoproteins for subsequent analysis of their transport itineraries and metabolism. Also, sterol-auxotroph cell lines and model organisms can use DHE or CTL as a sterol source and sterol transfer proteins can bind and transfer DHE and CTL between membranes similar to Chol (22). However, the unfavorable photophysical properties of DHE and CTL, which include UV absorption and UV fluorescence, low quantum yield, and high photobleaching propensity, make their use for advanced microscopy involving prolonged and repeated imaging of the sample or single molecule-based fluorescence fluctuation analysis very challenging. Organic dye-labeled analogs are suitable for microscopic imaging of Chol (23, 24), but despite their convenience, it is difficult to determine how well these analogs exhibit the properties of native Chol due to comparable sizes of the fluorophores and Chol.

Here, we use several organic dye-labeled Chol analogs, those labeled with 7-nitrobenz-2-oxa-1,3-diazol-4-yl (NBD) (25) and TopFluor (TF) (26) at different positions or with the dyes AbberiorStar512 and AbberiorStarRed via PEG linkers (27), and demonstrate their performance in different experimental modalities: *1*) their preference for more ordered membrane environments in phase-separated giant unilamellar vesicles (GUVs) and giant plasma membrane vesicles (GPMVs); *2*) their localization following intracellular trafficking in Niemann-Pick type C (NPC) disease cells; and *3*) their applicability in fluorescence correlation spectroscopy (FCS)-based measurements and super-resolution stimulated emission depletion (STED)-FCS-based measurements of membrane diffusion dynamics. Our data revealed strong differences between the analogs, with some indicating high performance in the membrane-based assay and others in the intracellular trafficking NPC-based assay, but none showing positive performance in all these experimental modalities.

MATERIALS AND METHODS

Chol analogs and lipids

The following molecules were used for visualizing Chol (Fig. 1): the Chol binding motifs filipin III (Cayman Chemical) and dansyl Chol (6-dansyl Chol, gift from Prof. Gerald Gimpl, Johannes Gutenberg University of Mainz), and the organic dye-tagged Chol analogs 22-NBD-Chol [22-(*N*-(7-nitrobenz-2-oxa-1,3-diazol-4-yl)amino)-23,24-bisnor-5-cholen-3β-ol, gift from Prof. Martin Hof, Prague, Czech Republic], 25-NBD-Chol {25-[*N*-[(7-nitro-2-1,3-benzoxadiazol-4-yl)methyl]amino]27-norcholesterol, gift from Prof. Martin Hof}, 3-C6-NBD-Chol {6-[(7-nitro-2,1,3-benzoxadial-4-yl)amino]cholest-5-en-3-ol, Cayman Chemical}, 3-C12-NBD-Chol {12-[(7-nitro-2,1,3-benzoxadiazol-4-yl)amino](3S,10R,13R)-3-methoxy-10,13-dimethyl-17-((R)-6-methylheptan-2-yl)-tetradecahydro-1H-cyclopenta[α]phenanthrene, Cayman Chemical}, TopFluor Chol (TF-Chol) [23-(dipyrromethemeboron difluoride)-24-norcholesterol, Avanti Polar Lipids, Alabaster, AL], and Star512-PEG-Chol and KK114-PEG-Chol with a PEG-2000 linker between Chol and the organic dye AbberiorStar512 (Abberior, Gottingen, Germany) and KK114 [or AbberiorStar Red, Abberior, synthesized as described previously (27)]. The fluorescent phospholipid analog, Atto647N-DOPE (Atto-Tec, Siegen, Germany), was used as a marker for liquid disordered (Ld) environments (28). Unlabeled 1,2-dioleoyl-*sn*-glycero-3-phosphocholine (DOPC), SM (*N*-stearoyl-D-erythro-sphingosylphosphorylcholine), and Chol were obtained from Avanti Polar Lipids.

Preparation of GUVs

GUVs were prepared via the electroformation method as described previously (29). Briefly, a lipid film was formed on a platinum wire from a 1 mg/ml lipid mix of DOPC:SM:Chol (2:2:1) containing approximately 0.01 mol% of Chol analog. GUVs were formed in 300 mM sucrose solution at 68°C. Ten hertz, 2 V alternating electric current was used for electroformation.

Preparation of supported lipid bilayers

Supported lipid bilayers (SLBs) were prepared as previously described using spin coating technique (30). DOPC lipid (1 mg/ml) dissolved in chloroform:methanol (1:1) was spread on piranha-cleaned glass. The coverslip was spun using a spin-coater (Chemat Technology) with 3,000 rpm for 40 s (30).

Cell culture

RBL-2H3 cells were maintained with 60% RPMI, 30% MEM, and 10% FCS (Sigma). M12 CHO cells ($NPC1^{-/-}$) and WT CHO cells ($CHO\text{-}NPC1^{+/+}$) cells were maintained in 90% DMEM (Sigma) and 10% FCS medium.

GPMVs

GPMVs were prepared as described previously (31). Briefly, RBL-2H3 cells seeded out on a 60 mm petri dish (~70% confluent) were washed with GPMV buffer [150 mM NaCl, 10 mM HEPES, 2 mM $CaCl_2$ (pH 7.4)] twice. Subsequently, 25 mM paraformaldehyde and 10 mM DTT (final concentrations) were added to the GPMV buffer, and 2 ml of this final buffer was added to the cells. The cells were incubated for 2 h at 37°C. Finally, GPMVs were collected by pipetting out the supernatant. Then, GPMVs were labeled by incubating 100 μl of GPMV suspension with 1 μl of 0.01 mg/ml [0.1 mg/ml for 6-dansyl-Chol (DChol) and filipin] fluorescent lipid analog for 15 min.

Confocal microscopy of GUVs and GPMVs

GUVs and GPMVs were imaged with a Zeiss LSM 780 confocal microscope in BSA-coated 8-well Ibidi glass chambers (#1.5). Filipin III and D-Chol were excited with 405 nm and emission was collected between 420 and 480 nm. NBD-, TF-, and Star512-labeled analogs were excited with 488 nm and emission collected between 505 and 550 nm. KK114- and Atto647N-labeled analogs were excited with 633 nm and emission collected by a LP 650

filter. The multi-track mode of the microscope was used to eliminate the cross-talk between channels.

Percent liquid ordered partitioning calculation

ImageJ-Line profile was used to calculate the preference of an analog to partition into the liquid ordered (Lo) environment of the GUVs and GPMVs, as described in (28, 31, 32). Briefly, a line was selected which crossed opposite sides of the equatorial plane of the GUVs or GPMVs having environments of different order (Lo and Ld) on opposite sides. Opposite sides were chosen to eliminate polarization artifacts in the readout from the laser excitation. The Lo partitioning coefficient (%Lo) was calculated as:

$$\%\mathrm{Lo} = \frac{F_{Lo}}{F_{Lo} + F_{Ld}} \cdot 100 \qquad \textit{(Eq. 1)}$$

where F_{Lo} and F_{Ld} are the detected fluorescence emission intensities in the Lo and Ld environment, respectively. If %Lo was >50%, a Chol analog was considered to prefer the Lo environment. We have shown negligible differences in the emission properties of the fluorescent dyes in the different environments in a previous work (28).

Fluorescent labeling and imaging of NPC cells

In contrast to all other analogs, filipin III staining was done on fixed cells. One microliter LysoTracker Red (Invitrogen; 100 μM stock) was added into 1 ml of complete cell medium (final concentration, 100 nM) and incubated for 2 h at 37°C. Cells were washed three times in medium without serum. One milliliter of 2% paraformaldehyde (in PBS) was added to the cells and the cells were incubated for 30 min at 4°C for fixation. Afterwards, the cells were washed three times with PBS. Finally, 0.05 mg/ml filipin III was added to the cells on a shaker in the dark for 30 min, and the cells were washed three times before imaging.

For labeling of live NPC1-deficient CHO cells with all other fluorescent Chol analogs, 1 μl LysoTracker Red (10 μM stock) was added into 1 ml of complete cell medium (final concentration, 10 nM) and incubated for 1 h at 37°C. Cells were washed three times in medium without serum, then incubated with approximately 5 μg/ml fluorescent Chol analogs in complete medium for 4 h at 37°C, and finally imaged on the confocal microscope, as described above. For simultaneous labeling of lysosomes, LysoTracker and fluorescent analogs were added at the same time and incubated for 4 h at 37°C.

The labeling procedure was the same irrespective of genetic status, i.e., diseased ($NPC1^{-/-}$) and healthy ($NPC1^{+/+}$) cells.

Imaging was again performed with a Zeiss LSM 780 confocal microscope with the excitation and detection wavelengths for the fluorescent Chol analogs chosen as for the GUV- and GPMV-based experiments. LysoTracker Red was excited with 543 nm and emission collected between 570 and 630 nm.

Colocalization analysis

Colocalization of the lysosome/late endosome marker, LysoTracker Red, and the fluorescent Chol analogs was analyzed from the confocal images of the doubly labeled NPC cells using the Coloc2 tool in FIJI (Fiji is just ImageJ, http://fiji.sc), and quantified by the Pearson correlation coefficient (PCC) (33). Values of PCC close to one indicate strong colocalization [as expected for disease ($NPC^{-/-}$) cells], while values of zero reveal minimal colocalization [values closer to zero are expected for healthy ($NPC^{+/+}$) cells due to the absence of a significant amount of Chol in lysosomes]. In order to compare the difference in colocalization between the diseased ($NPC1^{-/-}$) and healthy ($NPC1^{+/+}$) cells, we calculated the PCC for both cell lines [$PCC_{(NPC-/-)}$ and $PCC_{(NPC+/+)}$] and defined the parameter ΔPCC.

$$\Delta\mathrm{PCC} = \mathrm{PCC}_{(\mathrm{NPC}-/-)} - \mathrm{PCC}_{(\mathrm{NPC}+/+)} \qquad \textit{(Eq. 2)}$$

This parameter, for each analog, yields values of ΔPCC >> 0 in the case of stronger colocalization in the case of diseased ($NPC1^{-/-}$) compared with healthy ($NPC1^{+/+}$) cells, of ΔPCC ≈ 0 in the case of no difference, and of ΔPCC < 0 in the case of weaker colocalization in the case of diseased ($NPC1^{-/-}$) compared with healthy ($NPC1^{+/+}$) cells. The first case (ΔPCC >> 0) is expected and indicates proper characteristics of the Chol analog, while the latter two cases (ΔPCC ≤ 0) reveals wrong behavior of the Chol analog.

FCS and STED-FCS

FCS was carried out *1*) for the green emitting analogs on a Leica SP8 system equipped with a pulsed white-light-laser (80 ps pulse width, 80 MHz repetition rate) for fluorescence excitation at 488 nm, a 592 nm continuous-wave STED laser, an external avalanche photodiode (tau-SPAD) for fluorescence detection, and the PicoHarp detection electronics (Picoquant, Berlin, Germany) for calculation of the correlation function with the option for a software-integrated gated detection at 1 ns (30); and *2*) for the red-emitting analogs on an Abberior Resolft microscope (Abberior Instruments, Gottingen, Germany) equipped with an avalanche photodiode (SPCM-AQRH-13, Excelitas Techology), custom-extended with a pulsed 635 nm diode laser (Picoquant; 80 ps pulse width, repetition rate 80 MHz) for fluorescence excitation, a pulsed Ti:Sa laser (MaiTai, Spectra-Physics/Newport; 200 ps pulse width at microscope, 80 MHz repetition rate synchronizing the excitation laser) (34). Measurements were done on SLBs (30). Each measurement lasted 10 s. STED-FCS was carried out with the same setups. Cells or model membranes were loaded with 100 nM fluorescent molecules. Different STED powers were used for STED-FCS measurements.

The FCS data were fitted by custom-written software that is freely available [https://github.com/dwaithe/FCS_point_correlator (35)], using a one-component two-dimensional diffusion and one-triplet model (30),

$$G(t_c) = G(0)\frac{1}{\left(1+\frac{\tau}{t_D}\right)^{-1}}\left(1 - T + T\,e^{-\frac{\tau_c}{t_T}}\right) \qquad \textit{(Eq. 3)}$$

with correlation function $G(t_c)$ and amplitude $G(0)$, correlation time t_c, average transit time τ_D, triplet fraction T, and triplet correlation time τ_T. Together with the average total count-rate $<F>$, the amplitude $G(0)$ allows estimating the single-molecule brightness [or counts per molecule (*cpm*)]

$$cpm = G(0) < F > \qquad \textit{(Eq. 4)}$$

In this report, the data presented was fitted in the time window of t_c = 0.001 − 200 ms. Confocal measurements were used to determine T, and triplet correlation time τ_T, which were then fixed during further fitting. The quality of each fit was visually inspected.

In the case of the STED-FCS data, the transit time, τ_D, was used to calculate the diameter, d (full-width-at-half-maximum), of the effective observation spot at different STED powers P_{STED}.

$$d(P_{STED}) = d(P_{STED} = 0)\sqrt{\frac{\tau_D(P_{STED})}{\tau_D(P_{STED} = 0)}} \qquad \textit{(Eq. 5)}$$

JOURNAL OF LIPID RESEARCH ASBMB

Here, $d(P_{STED})$ and $\tau_D(P_{STED})$ are the diameter of the observation spot and the average transit time at the STED power, P_{STED}, and $d(P_{STED} = 0)$ and $\tau_D(P_{STED} = 0)$ the respective parameters at confocal recordings, where the diameter of the confocal spot [$d(P_{STED} = 0)$ = 200 nm for 488 nm and 240 nm for 635 nm excitation] has been determined from imaging fluorescent beads or from theory (36). Shortening of the transit time τ_D due to photobleaching from the STED laser is unlikely, as has been shown by several control measurements before, i.e., the decrease in d with STED power P_{STED} is not a result of photobleaching by the STED laser [e.g., (37, 38)]. While such photobleaching would potentially prevent the detection of slowly moving fluorescent molecules, because they would photobleach before entering the effective observation spot, a reduction of the transit time τ_D due to photobleaching from laser irradiation has been shown to be more prominent for confocal recordings, i.e., without the STED laser (38).

RESULTS AND DISCUSSION

We used the following fluorescent Chol analogs for their performance in three different assays testing their potential to measure membrane and intracellular trafficking dynamics: the Chol binding fluorescent dye, filipin III (12, 39), and Chol analogs tagged with the organic dye, dansyl (DChol labeled at the steroid backbone) (40), NBD (22-NBD-Chol labeled at position 22 of the side alkyl chain, 25-NBD-Chol labeled at position 25 of the side alkyl chain, 3-C6-NBD-Chol and 3-C12-NBD-Chol, both labeled at position 3 (i.e., at the 3β-OH group) via a C6- and C12-linker, respectively), BODIPY-derived TF-Chol (labeled at position 24 of the side alkyl chain), AbberiorStar512 (Star512-PEG-Chol) and KK114 (27) (or Abberior Star Red) (KK114-PEG-Chol) labeled at position 3 via a PEG2000-linker. The structures of the Chol analogs are depicted in **Fig. 1**. Labeling at the alkyl chain is usually preferred over attachment of the dye to the 3β-OH group, because it has been indicated that the respective –OH group may play important roles in Chol functionality and interactions (41). Labeling lipids with linkers has previously been introduced as a way to decrease the influence of the dye label on the lipids' characteristics (27, 42), as done with the C6- and C12-linkers in 3-C6- and 3-C12-NBD-Chol, or the even longer PEG2000-linkers, in the case of Star512- and KK114-PEG-Chol. We have not included measurements on DHE and CTL here due to the necessity to use UV irradiation, as well as due to their low brightness and low photostability, which make them unfavorable for advanced microscopy.

Partitioning in phase-separated model membranes

The organization and dynamics of molecules in the plasma membrane of the living cell play an important role in many cellular signaling events. Here, a crucial role is dedicated to the role of Chol, because many experiments indicated that signaling varies with varying Chol levels (43). Specific attention has been given to the lipid raft or nanodomain concept, which postulates transient, lipid-dependent, and Chol-rich domains as an organizational principle of the plasma membrane, compartmentalizing cellular signaling (2, 7). Various proteins and lipids are thought to assemble within such small domains, thereby locally increasing the molecular order. An open question is how coordinated and active lipids reorganize into such structures. Unfortunately, due to their transient state and small size, lipid rafts have so far not directly been observed in the living cell. Consequently, membrane systems such as GUVs or GPMVs are often taken as a model to investigate lipid membrane ordering and, thus, potential lipid raft properties, especially because these model membrane systems tend to separate into phases of more ordered (Lo) and disordered (Ld) environments (44, 45). Besides indicating coordinated lipid behavior, the Lo environment, specifically, due to its high molecular order, has been thought to reveal some physical properties of lipid rafts (45). While GUVs are fully artificial membrane vesicles, usually comprised of a ternary mixture of Chol and unsaturated and saturated lipids, GPMVs are derived from the plasma membrane of living cells, thus containing its lipid and protein diversity (32, 46). Despite several recent contradictory reports (20, 47–49), Chol has been given an essential role in this lipid raft concept (2). This is mainly because Chol not only fluidizes the ordered environment, but also orders the disordered environment, and Chol-dependent density fluctuations are supposed to manifest at the nanoscale, i.e., beyond the resolution limit of classical imaging approaches (50, 51). Thus, it is of great interest how Chol behaves in phase-separated membranes such as GUVs and GPMVs, specifically which environment (Lo or Ld) it prefers. The dominating opinion is that Chol enriches in the Lo domains because intrinsically fluorescent Chol analogs (DHE and CTL) were found to partition with high preference into the Lo phase in model membranes (7, 19, 52). However, a recent hypothesis suggested that Chol is evenly distributed between domains (49). Studies using advanced fluorescence microscopy are hampered by the necessity to use organic dye labels, which, due to their size, usually prevent the labeled lipids or Chol from efficiently entering the Lo environment (28). We, therefore, investigated the partitioning characteristics of the different fluorescent Chol analogs in both phase-separated GUVs and GPMVs.

For this purpose, we labeled the membrane of phase-separated GUVs [DOPC:SM:Chol (2:2:1)] and RBL-2H3 cell-derived GPMVs with the different fluorescent Chol analogs, and imaged the equatorial plane of the vesicles using confocal microscopy, as representatively shown in **Fig. 2A** for filipin III and 3-C6-NBD-Chol. We used the fluorescent phospholipid analog, Atto647N-DOPE, as a marker for the Ld environment (28), and for each Chol analog quantified the preference of entering the Lo environment by calculating the partitioning coefficient %Lo from the fluorescence intensities detected for the Chol analogs in the Ld and Lo environment using equation 1. Values of %Lo = 0 and 100 indicate the extreme cases of no partitioning and complete partitioning into the Lo environment, respectively. Figure 2B compares values of the partitioning coefficient %Lo for the different Chol analogs. Due to the compositional complexity, the molecular

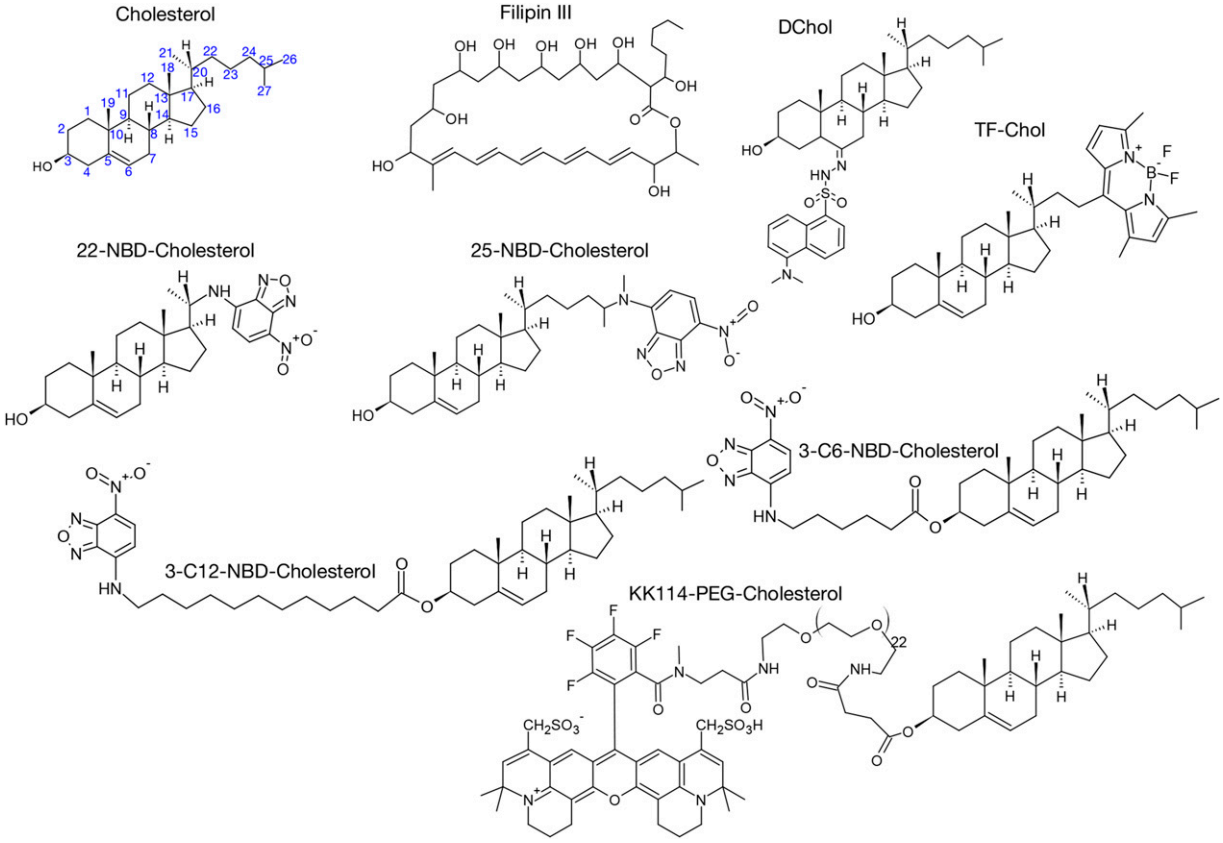

Fig. 1. Molecular structures of Chol and the employed fluorescent Chol analogs. The structure of Star512-PEG-Chol is not shown here due to the missing knowledge of the structure of the AbberiorStar 512 dye; but the principle structure is very similar to that of KK114-PEG-Chol.

order in the Lo environment and, thus, the order difference between Lo and Ld environments is less in GPMVs than in GUVs, leading, in general, to an easier access of more ordered environments and, consequently, to larger %Lo values in GPMVs compared with GUVs (28, 51, 53). The Chol binding probe, filipin III, shows the highest preference for the Lo environment in both GUVs and GPMVs with %Lo values of up to 80% (Fig. 2A, B). This observation is in accordance with earlier studies using CTL or DHE (19), and it provides strong evidence for ordered domain enrichment of native Chol in phase-separated model membranes. Filipin III is an intrinsically fluorescent compound that binds Chol (12, 39), and it is obviously expected to occupy less space than the Chol analogs carrying an additional similarly sized organic dye (28, 54). Consequently, it is not surprising that the %Lo values of all other dye-tagged analogs are smaller. Yet, TF-Chol and the PEG2000-linked Star512- and KK114-PEG-Chol revealed almost similar Lo preference with values of %Lo $\geq$ 50% in both GUVs and GPMVs, as indicated before (21, 26, 28, 42, 55). All other analogs, i.e., those labeled with NBD or dansyl, mostly avoided the more ordered environments

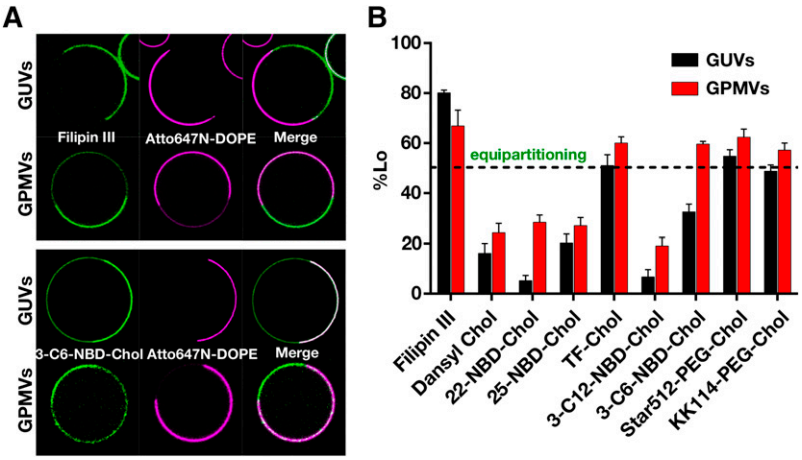

Fig. 2. Partitioning characteristics of the fluorescent Chol analogs in phase-separated GUVs and GPMVs. A: Representative confocal images of the equatorial plane of GUVs and GPMVs for filipin III (top panel) and 3-C6-NBD-Chol (bottom panel): fluorescent Chol analog (green, left panels), fluorescent Ld-marker Atto647N-DOPE (red, middle panels), and merged images (right panels) (image size is 40 × 40 μm for GUVs and 20 × 20 μm for GPMVs). B: The %Lo values calculated (equation 1) from the confocal images as representatively shown in (A) for all investigated Chol analogs (black, GUVs; red, GPMVs). The dashed line indicates equal partitioning between Lo and Ld (%Lo = 50%). Average and SD (error bars) values obtained from >10 measurements on different vesicles prepared on at least three different days.

with values of down to %Lo < 10% in GUVs. On first sight, this seems to be surprising, because both dyes are smaller in size than the other dyes, indicating, in this case, a size-independent property to be responsible for avoidance of highly packed membrane regions. It is known that NBD has the tendency to back-loop toward the membrane interface (56, 57), hence, the side-chain tagged NBD-Chol analogs will, in turn, require more space in the membrane, which can squeeze the analogs out of the ordered phase (54). Our data shows that insertion of the long PEG2000 linkers between the Chol and a dye label improves the partitioning characteristics of the respective analog (as for Star512- and KK114-PEG-Chol). It is thought that due to the long PEG-linker, the dye label is excluded from the membrane (55). Yet, C6 and C12 carbon linkers, as introduced for the C6- and C12-NBD-Chol analogs, seem not to be sufficient. However, it is worth noting that, similar to TF- and PEG-linker Chol analogs, 3-C6-NBD-Chol shows significant %Lo (60%) in GPMVs compared with longer linker 3-C12-NBD-Chol (Fig. 2A, lower panel). Thus, it is not trivial to draw a general rule to predict the partitioning of an organic dye-labeled analog.

Intracellular trafficking: NPC1-null cells

Proper cellular function of Chol relies on its nonbiased insertion and localization into the plasma membrane (as outlined in the above example) and on its correct intracellular trafficking, which are both related. Trafficking of Chol between intracellular organelles and the cell membrane is tightly regulated (58). Shortcomings in these pathways may result in severe metabolic disorders. In NPC disease, caused by mutations in the genes coding either for the NPC1 or the NPC2 proteins, Chol trafficking from late endosomes and lysosomes is impaired and Chol is "stored" in late endosomes (59, 60). For NPC1-deficient cells, not only transport of lipoprotein-derived Chol from endosomes is impaired, but also normal circulation of de novo synthesized- and plasma-membrane-derived Chol is affected (61, 62). In fact, in a Chinese hamster ovarian cell line with mutated NPC1 protein, normal trafficking of DHE and TF-Chol between the plasma membrane and recycling endosomes is disturbed, and the sterol probes were found to accumulate in lysosomal storage organelles over several hours (62, 63). We used the same model cell system to determine the trafficking itineraries of the Chol analogs in this study. NPC phenotyping has previously been performed by visualizing the localization of cellular Chol using filipin III (60, 64). Therefore, we first imaged healthy ($NPC1^{+/+}$) and diseased ($NPC1^{-/-}$) NPC cells stained with filipin III and the lysosomal marker LysoTracker using confocal microscopy, allowing us to examine the colocalization of filipin and LysoTracker. As expected, we observed a notable difference in the colocalization between $NPC1^{+/+}$ and $NPC1^{-/-}$ cells (**Fig. 3A**). While filipin mainly stained the plasma membrane of $NPC1^{+/+}$ cells, it was mainly in the late endosomes/lysosomes of $NPC1^{-/-}$ cells. To quantify the extent of colocalization between Chol and LysoTracker, we calculated the PCC from their respective fluorescence images, which is one for complete and zero for no colocalization. As expected, the PCC was close to one for $NPC1^{-/-}$ and almost zero for $NPC1^{+/+}$ cells (Fig. 3B). Calculation of the difference parameter ΔPCC in PCC values (equation 2) further revealed this change in colocalization, because larger values of ΔPCC indicate the expected accumulation of Chol in lysosomes in $NPC1^{-/-}$ cells, while values of ΔPCC around or even below zero indicate no change or an unexpected change.

While these results show that filipin is a robust reporter to observe Chol accumulation in NPC disease, it is not applicable to living cells because the cells need to be fixed before labeling, precluding live-cell observations. In contrast, all other Chol analogs used in this study could be employed in live-cell investigations; their colocalization with lysosomes is also depicted in Fig. 3. Unfortunately, the values of Pearson coefficients, PCC and ΔPCC, show less appropriate trafficking properties for all of the live-cell adaptable probes. Specifically, dansyl-Chol, TF-Chol, Star512-PEG-Chol, and KK114-PEG-Chol were the least sensitive analogs to NPC1 status. Among them, the inappropriate properties of TF-Chol are probably the most surprising ones because TF-Chol is considered as one of the most suitable Chol analogs at the present time (26, 63). It accumulates in spherical structures inside the cell, which do not colocalize with LysoTracker (supplementary Fig. 1). It is likely that these structures resemble lipid droplets, in which TF-Chol has been shown to partition preferentially compared with other sterol probes, such as DHE, filipin, or Raman-active phenyl-diyne-Chol (21, 65, 66). All NBD-labeled analogs, specifically, 3-C6-NBD-Chol and 25-NBD-Chol, showed values of ΔPCC comparable to filipin (Fig. 3A, B), making these the most appropriate candidates for reporting live-cell trafficking. Close comparison of the PCC values of these NBD-tagged analogs suggests that the labeling position is essential for the dynamics of the analog. For example, while 25-NBD-Chol was to a large extent localized to lysosomes in $NPC1^{-/-}$ cells, 22-NBD was much less colocalized with lysosomes in $NPC1^{-/-}$ cells (supplementary Fig. 3).

Despite the promising properties of Star512-PEG-Chol and KK114-PEG-Chol with regard to plasma membrane organization, only a small fraction of these probes gets internalized; rather, they were still enriched in the plasma membrane even after several hours of incubation (supplementary Fig. 2). Interestingly, the internalized pool of PEG-containing Chol probes colocalized with late endosomes/lysosomes to a similar extent in both $NPC1^{+/+}$ and $NPC1^{-/-}$ cells. Related to this, in separate experiments (carried out in baby hamster kidney cells), we observed that KK114-PEG-Chol strongly colocalized with DHE in the plasma membrane and after some time in a few endocytic vesicles (supplementary Fig. 4A). In those baby hamster kidney cells, we also found a distinctive trafficking of DHE and TF-Chol to the perinuclear endocytic recycling compartment (ERC), a major sterol storage organelle in healthy mammalian cells (supplementary Fig. 4B) (67). To a certain extent, the low fraction of internalized KK114-PEG-Chol also targeted the ERC (supplementary Fig. 4B).

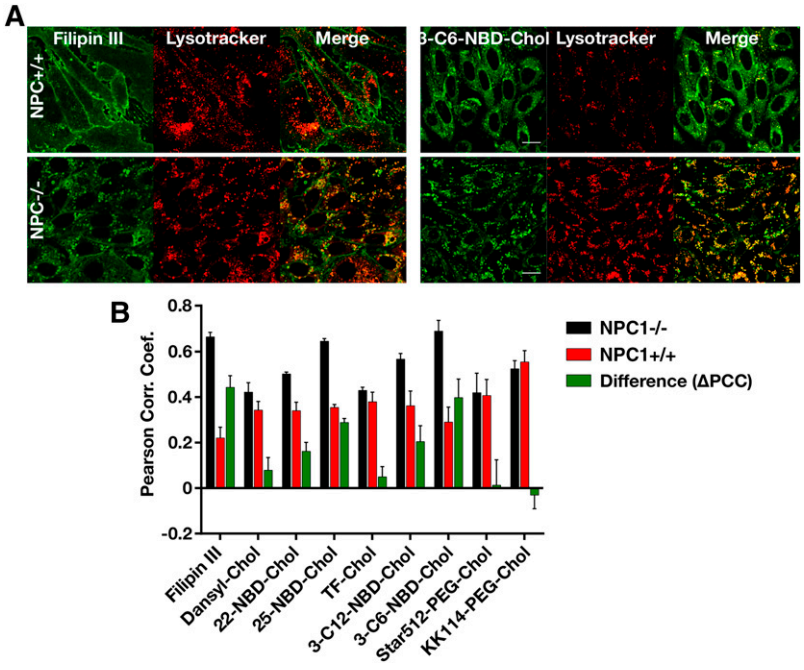

Fig. 3. Characteristics of trafficking of the Chol analogs in NPC disease: healthy $NPC1^{+/+}$ and diseased $NPC1^{-/-}$ cells. A: Representative confocal images of filipin (left panels) and 3-C6-NBD (right panels) and LysoTracker-stained $NPC1^{+/+}$ (upper panels) and $NPC1^{-/-}$ cells (lower panels), as labeled. Both analogs show an expected behavior: colocalization of Chol analogs with lysosomes in disease $NPC1^{-/-}$ cells and no colocalization in $NPC1^{+/+}$ cells. B: Quantification of colocalization of LysoTracker and Chol analogs using the PCC, which is one for complete and zero for no colocalization, and the difference parameter ΔPCC in PCC values between $NPC1^{+/+}$ and $NPC1^{-/-}$ cells, which takes larger values for the expected change in PCC values and is close to zero for no observable change in colocalization.

For DHE and TF-Chol, and also for Chol, it has been shown that part of the sterol transport between the plasma membrane and the ERC takes place by a nonvesicular mechanism (67, 68). This transport mode requires fast trans-bilayer migration of the sterol, and indeed, the majority of DHE and CTL has been shown to reside after membrane labeling on the inner leaflet of the plasma membrane (69). We suggest that the large-sized PEG-linker in KK114-PEG-Chol and Star512-PEG-Chol prevents sterol flip-flop and, therefore, only allows for vesicular uptake in these cells. Accordingly, their enrichment in Chol-containing organelles, such as the ERC in healthy cells or the lysosomal storage organelles in NPC cells, is lower than that of analogs with fast trans-bilayer movement (17, 70).

FCS on Chol analogs

Fluorescence microscopy and spectroscopy are important techniques for observing molecular organization and dynamics in living cells, as indicated in the two previous examples for the localization of the Chol analogs. Besides the spatial localization, the diffusion and interaction dynamics are also parameters essential to the function of Chol. FCS is a useful tool for investigating diffusion and interaction dynamics of fluorescently labeled molecules (71–74). In FCS, temporal fluctuations in the detected fluorescence due to molecular transits through the microscope's observation spot are analyzed to, for example, determine average transit times and molecular mobility. Crucial parameters for accurate fluorescence microscopy and spectroscopy, especially FCS measurements, are the brightness and photostability of the fluorescent label (75). While a limited brightness results in noisy data, low photostability impedes the correct determination of molecular organization and dynamics; for example, in FCS, a limited photostability might result in the loss of fluorescence before the molecules have fully traversed the observation spot, thus leading to a bias in the acquired transit time (30).

To check the applicability of our fluorescent Chol analogs in FCS, we recorded FCS data of the analogs diffusing in a SLB (100% DOPC on acid-cleaned glass). We selected only TF-Chol, Star512-PEG-Chol, KK114-PEG-Chol, and the 22-NBD-Chol for FCS analysis. Filipin III, as well as dansyl-Chol, did not give rise to any FCS curve, indicating their inappropriateness for these kinds of measurements due to low brightness and photostability. In the case of NBD, we only present the data of 22-NBD-Chol as a representative of all the NBD analogs, because we did not experience a remarkable difference between them. Also note that, while TF-Chol, Star512-PEG-Chol, and NBD-Chol were all excited at 488 nm, KK114-PEG-Chol was excited at 635 nm. From the FCS data, we could determine values of the average transit times, τ_D (equation 3), and brightness or *cpm* (equation 4). **Figure 4A, B** compares the brightness values recorded at an excitation power of 5 μW. Of all 488 nm excitable analogs, TF-Chol showed the highest brightness, followed by Star512-PEG-Chol and a very low brightness for the NBD-Chol analogs. KK114-PEG-Chol (Fig. 4B) showed an even 5-fold larger brightness than TF-Chol at this excitation power, albeit at a different excitation wavelength, as already indicated. Figure 4C, D depicts the transit times, τ_D, determined for increasing excitation powers. A decrease in τ_D for large excitation powers indicates enhanced photobleaching, i.e., low photostability, because the fluorescent molecules turn dark prior leaving the observation spot (30). Here, all analogs except the NBD-Chol showed a satisfactory performance for excitation powers of up to 40 μW, while in the case of NBD-Chol, values of transit times had already dropped off at values of 5–10 μW. In a nutshell, only TF-Chol, Star512-PEG-Chol, and especially KK114-PEG-Chol were suitable for FCS measurements, while filipin III, dansyl-Chol, and the NBD-labeled probes

JOURNAL OF LIPID RESEARCH ASBMB

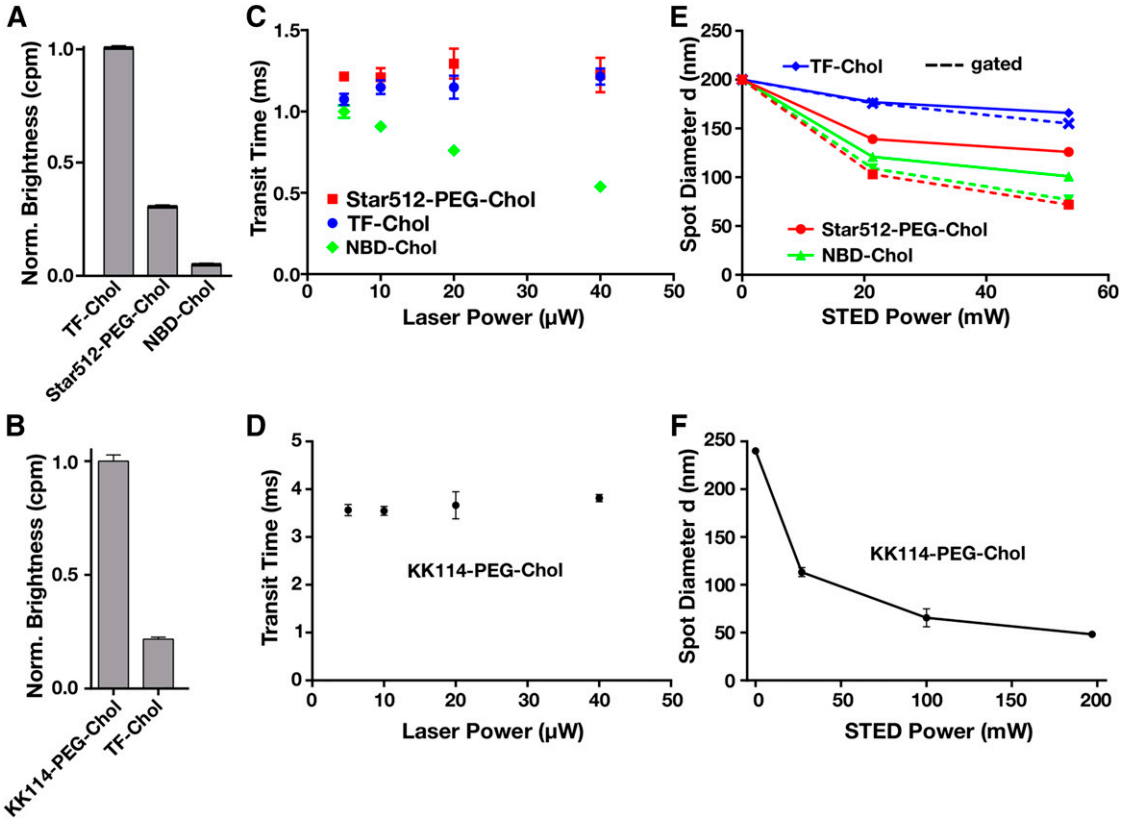

Fig. 4. FCS and STED-FCS recordings of Chol analogs diffusing in a SLB (100% DOPC on cleaned glass). NBD-Chol shows the results of 22-NBD-Chol as a representative of all NBD-tagged Chol analogs. A, B: Relative values of brightness (or *cpm*) recorded at 5 μW: normalization to TF-Chol (upper panel) (A) and KK114-PEG-Chol (lower panel) (B). C, D: Relative decrease in transit time (τ_D) with increasing excitation power (normalization to recordings at 5 μW) for green-emitting dyes (C) and red-emitting KK114-PEG-Chol (D). E, F: Decrease of the diameter of the observation spot with increasing STED power (P_{STED}) as obtained from the transit time [$\tau_D(P_{STED})$] using equation 5 for green-emitting dyes (E) and red-emitting KK114-PEG-Chol (F). For the 488 nm excited analogs (E), straight and dashed lines denote nongated and gated detection modes, respectively.

were shown not to be useful. Not surprisingly, TF-Chol and, specifically, KK114-PEG-Chol have been used in previous FCS-based measurements (42, 76).

Super-resolution STED recordings

Recent developments in optical imaging have seen the rise of several super-resolution optical microscopy techniques. Using transitions between different states of a fluorescent label (e.g., a dark and a bright state) and thereby modulating the fluorescence (e.g., reversibly inhibiting fluorescence emission), these techniques allow the observation of cellular structures at a spatial resolution below the diffraction limit of ~200 nm of conventional microscopes (77). The first of this kind was STED microscopy (77), where the size of the effective observation spot is reduced by the addition of a STED laser inducing reversible inhibition of fluorescence emission through stimulated emission. A unique feature of STED microscopy is the possibility of tuning the size of the effective observation spot through the intensity of the STED laser, as well as the straightforward ability of combining it with FCS. Through recording FCS data at different observation spot sizes (with down to $d < 60$ nm diameters), STED-FCS realizes a detailed disclosure of molecular diffusion modes and interactions (37, 78). Increasing the sensitivity of FCS, STED-FCS also increases the demands on brightness and photostability of a fluorescent label. On one hand, reduced observation spot sizes yield a smaller amount of total photons from a traversing single molecule. On the other hand, the additional STED laser irradiation might induce additive photobleaching (30, 79). We checked the performance of those Chol analogs that we had already tested in the conventional FCS recordings for their usefulness for STED-FCS.

We incorporated the Chol analogs into an SLB, as before, and measured their average transit times (τ_D) as we increased the power (P_{STED}) of the STED laser. From theory, the diameter (d) of the observation spot decreases with increasing P_{STED} ($d \sim C/\sqrt{P_{STED}}$, with C depending on, among other parameters, the photophysical properties of the fluorescent label) (79). Figure 4E, F plots the dependencies [$d(P_{STED})$] obtained for the different Chol analogs. In all cases, we observed an expected decrease of d with P_{STED}, differing between the different probes. Steep declines of $d(P_{STED})$ entail reaching small observation spot sizes at low STED powers, thereby minimizing the laser irradiation on the sample. Shortening of the transit time (τ_D) due to photobleaching from the STED laser is unlikely, as has been shown previously by several control measurements, i.e., the decrease in d with STED power

(P_{STED}) is not a result of photobleaching by the STED laser (37, 38). Anticipated steep declines were revealed for KK114-PEG-Chol and Star512-PEG-Chol, making them the most appropriate for STED-FCS recordings. In contrast, TF-Chol did not show a significant decrease of $d(P_{STED})$. Note that in the case of the 488 nm excitable Chol analogs (e.g., Star512-PEG-Chol), where we employed a continuous-wave (CW) STED laser (instead of the pulsed STED laser following 635 nm excitation as for KK114-PEG-Chol), the steepness of the decline was further increased using a gated detection scheme, as expected (30). While we could straightforwardly reach diameters of down to 50 nm for both KK114-PEG-Chol and Star512-PEG-Chol, as usually employed in STED-FCS recordings (42), with TF-Chol we could, even with gated detection, hardly reach 150 nm, at least with $P_{STED} < 60$ mW of 592 nm CW STED laser light. Previous STED-FCS recordings of TF-Chol had to use gated detection in conjunction with >100 mW of 577 nm CW STED laser light to reach $d < 100$ nm (76). A current study has therefore employed KK114-PEG-Chol for STED-FCS membrane studies (42). Surprisingly, we realized rather good STED performance with NBD-Chol also. Unfortunately, its characteristics with regard to photobleaching in confocal FCS recordings also disfavor the NBD analogs for STED-FCS recordings.

CONCLUSION

Chol is of great importance in cellular structure and function. Therefore, it is crucial to visualize Chol in cells, which is often done using fluorescent Chol analogs. Here, we analyzed various Chol analogs for their potential to image cellular Chol localization and dynamics. We tested their localization, i.e., their partitioning characteristics in phase-separated model membranes, their intracellular trafficking in NPC1 disease cells, and their performance in confocal and advanced super-resolution FCS, for probing plasma-membrane dynamics. The Chol analogs performed very differently in these three assays. While Chol analogs with fluorescent dye tags separated by a long PEG-linker proved superior for testing different membrane phases, as well as for use in FCS and STED-FCS measurements, they did not perform well in intracellular trafficking experiments. Vice versa, NBD-labeled Chol analogs showed satisfactory performance in intracellular trafficking, but exhibited poor performance in phase partitioning (except 3-C6-NBD-Chol, which partitioned into the ordered domains in GPMVs) and FCS experiments. TF-Chol, an analog that had so far been regarded to perform well in cellular assays, did not behave appropriately in the intracellular trafficking assay and did not show good performance in STED-based experiments, yet indicated good properties for testing different membrane phases.

It is important to note that fluorescently labeled Chol analogs carry a similar-sized fluorophore as Chol, thus behavior of these analogs might be greatly ruled by the attached fluorophore. Thus, in principle, natural Chol analogs, such as DHE and CTL, are better options to mimic Chol. However, we kept them out of the scope of this study due to their fairly poor photo-physical properties (such as UV absorption and fluorescence, low quantum yield, high photobleaching). Such properties make UV-optimized optics in the excitation path of a conventional wide field microscope or multiphoton excitation and UV-sensitive detectors (which are all not easily available in cell biological laboratories) requirements for their visualization (80). In addition, their low brightness and high bleaching propensity make DHE and CTL unsuitable for single molecule studies or STED-based experiments, which were some important criteria we assessed in our analysis.

Overall, this study provides a useful guide for appropriate use of Chol analogs in advanced live subcellular imaging applications.

The authors acknowledge support by Dr. Christoffer Lagerholm as well as the Wolfson Imaging Centre Oxford.

REFERENCES

1. Maxfield, F. R., and I. Tabas. 2005. Role of cholesterol and lipid organization in disease. *Nature.* **438:** 612–621.
2. Simons, K., and E. Ikonen. 1997. Functional rafts in cell membranes. *Nature.* **387:** 569–572.
3. Edwards, P. A., and J. Ericsson. 1999. Sterols and isoprenoids: signaling molecules derived from the cholesterol biosynthetic pathway. *Annu. Rev. Biochem.* **68:** 157–185.
4. Furuchi, T., and R. G. W. Anderson. 1998. Cholesterol depletion of caveolae causes hyperactivation of extracellular signal-related kinase (ERK). *J. Biol. Chem.* **273:** 21099–21104.
5. Lewis, P. M., M. P. Dunn, J. A. McMahon, M. Logan, J. F. Martin, B. St-Jacques, and A. P. McMahon. 2001. Cholesterol modification of sonic hedgehog is required for long-range signaling activity and effective modulation of signaling by Ptc1. *Cell.* **105:** 599–612.
6. Porter, J. A., K. E. Young, and P. A. Beachy. 1996. Cholesterol modification of hedgehog signaling proteins in animal development. *Science.* **274:** 255–259.
7. Silvius, J. R. 2003. Role of cholesterol in lipid raft formation: lessons from lipid model systems. *Biochim. Biophys. Acta.* **1610:** 174–183.
8. Schroeder, F., H. Huang A. L. McIntosh, B. P. Atshaves, G. G. Martin, and A. B. Kier. 2010. Caveolin, sterol carrier protein-2, membrane cholesterol-rich microdomains and intracellular cholesterol trafficking. *Subcell. Biochem.* **51:** 279–318.
9. Mizuno, H., M. Abe, P. Dedecker, A. Makino, S. Rocha, Y. Ohno-Iwashita, J. Hofkens, T. Kobayashi, and A. Miyawaki. 2011. Fluorescent probes for superresolution imaging of lipid domains on the plasma membrane. *Chem. Sci.* **2:** 1548–1553.
10. Pourmousa, M., T. Rog, R. Mikkeli, I. Vattulainen, L. M. Solanko, D. Wustner, N. H. List, J. Kongsted, and M. Karttunen. 2014. Dehydroergosterol as an analogue for cholesterol: why it mimics cholesterol so well-or does it? *J. Phys. Chem. B.* **118:** 7345–7357.
11. Robalo, J. R., A. M. T. Martins do Canto, A. J. Palace Carvalho, J. P. Prates Ramalho, and L. M. S. Loura. 2013. Behavior of fluorescent cholesterol analogues dehydroergosterol and cholestatrienol in lipid bilayers: a molecular dynamics study. *J. Phys. Chem. B.* **117:** 5806–5819.
12. Gimpl, G., and K. Gehrig-Burger. 2007. Cholesterol reporter molecules. *Biosci. Rep.* **27:** 335–358.
13. Arthur, J. R., K. A. Heinecke, and T. N. Seyfried. 2011. Filipin recognizes both GM1 and cholesterol in GM1 gangliosidosis mouse brain. *J. Lipid Res.* **52:** 1345–1351.
14. Tserentsoodol, N., J. Sztein, M. Campos, N. V. Gordiyenko, R. N. Fariss, J. W. Lee, S. J. Fliesler, and I. R. Rodriguez. 2006. Uptake of cholesterol by the retina occurs primarily via a low density lipoprotein receptor-mediated process. *Mol. Vis.* **12:** 1306–1318.
15. Albert, A. D., J. E. Young, and P. L. Yeagle. 1996. Rhodopsin-cholesterol interactions in bovine rod outer segment disk membranes. *Biochim. Biophys. Acta.* **1285:** 47–55.

16. Yeagle, P. L., A. D. Albert, K. Boeszebattaglia, J. Young, and J. Frye. 1990. Cholesterol dynamics in membranes. *Biophys. J.* **57:** 413–424.
17. John, K., J. Kubelt, P. Muller, D. Wustner, and A. Herrmann. 2002. Rapid transbilayer movement of the fluorescent sterol dehydroergosterol in lipid membranes. *Biophys. J.* **83:** 1525–1534.
18. Mukherjee, S., X. H. Zha, I. Tabas, and F. R. Maxfield. 1998. Cholesterol distribution in living cells: Fluorescence imaging using dehydroergosterol as a fluorescent cholesterol analog. *Biophys. J.* **75:** 1915–1925.
19. Garvik, O., P. Benediktson, A. C. Simonsen, J. H. Ipsen, and D. Wustner. 2009. The fluorescent cholesterol analog dehydroergosterol induces liquid-ordered domains in model membranes. *Chem. Phys. Lipids.* **159:** 114–118.
20. Wüstner, D. 2008. Free-cholesterol loading does not trigger phase separation of the fluorescent sterol dehydroergosterol in the plasma membrane of macrophages. *Chem. Phys. Lipids.* **154:** 129–136.
21. Wüstner, D., L. Solanko, E. Sokol, O. Garvik, Z. Li, R. Bittman, T. Korte, and A. Herrmann. 2011. Quantitative assessment of sterol traffic in living cells by dual labeling with dehydroergosterol and BODIPY-cholesterol. *Chem. Phys. Lipids.* **164:** 221–235.
22. Wüstner, D., and K. Solanko. 2015. How cholesterol interacts with proteins and lipids during its intracellular transport. *Biochim. Biophys. Acta.* **1848:** 1908–1926.
23. Wüstner, D. 2007. Fluorescent sterols as tools in membrane biophysics and cell biology. *Chem. Phys. Lipids.* **146:** 1–25.
24. Boldyrev, I. A., X. H. Zhai, M. M. Momsen, H. L. Brockman, R. E. Brown, and J. G. Molotkovsky. 2007. New BODIPY lipid probes for fluorescence studies of membranes. *J. Lipid Res.* **48:** 1518–1532.
25. Ramirez, D. M., W. W. Ogilvie, and L. J. Johnston. 2010. NBD-cholesterol probes to track cholesterol distribution in model membranes. *Biochim. Biophys. Acta.* **1798:** 558–568.
26. Ariola, F. S., Z. Li, C. Cornejo, R. Bittman, and A. A. Heikal. 2009. Membrane fluidity and lipid order in ternary giant unilamellar vesicles using a new bodipy-cholesterol derivative. *Biophys. J.* **96:** 2696–2708.
27. Honigmann, A., V. Mueller, S. W. Hell, and C. Eggeling. 2013. STED microscopy detects and quantifies liquid phase separation in lipid membranes using a new far-red emitting fluorescent phosphoglycerolipid analogue. *Faraday Discuss.* **161:** 77–89.
28. Sezgin, E., I. Levental, M. Grzybek, G. Schwarzmann, V. Mueller, A. Honigmann, V. N. Belov, C. Eggeling, U. Coskun, K. Simons, et al. 2012. Partitioning, diffusion, and ligand binding of raft lipid analogs in model and cellular plasma membranes. *Biochim. Biophys. Acta.* **1818:** 1777–1784.
29. García-Sáez, A. J., D. C. Carrer, and P. Schwille. 2010. Fluorescence correlation spectroscopy for the study of membrane dynamics and organization in giant unilamellar vesicles. *Methods Mol. Biol.* **606:** 493–508.
30. Clausen, M. P., E. Sezgin, J. Bernardino de la Serna, D. Waithe, B. C. Lagerholm, and C. Eggeling. 2015. A straightforward approach for gated STED-FCS to investigate lipid membrane dynamics. *Methods.* **88:** 67–75.
31. Sezgin, E., H-J. Kaiser, T. Baumgart, P. Schwille, K. Simons, and I. Levental. 2012. Elucidating membrane structure and protein behavior using giant plasma membrane vesicles. *Nat. Protoc.* **7:** 1042–1051.
32. Levental, I., D. Lingwood, M. Grzybek, U. Coskun, and K. Simons. 2010. Palmitoylation regulates raft affinity for the majority of integral raft proteins. *Proc. Natl. Acad. Sci. USA.* **107:** 22050–22054.
33. Adler, J., and I. Parmryd. 2010. Quantifying colocalization by correlation: the Pearson correlation coefficient is superior to the Mander's overlap coefficient. *Cytometry A.* **77:** 733–742.
34. Clausen, M. P., S. Galiani, J. B. de la Serna, M. Fritzsche, J. Chojnacki, K. Gehmlich, B. C. Lagerholm, and C. Eggeling. 2013. Pathways to optical STED microscopy. *NanoBioImaging.* **1:** 1–12.
35. Waithe, D., M. P. Clausen, E. Sezgin, and C. Eggeling. FoCuS-point: software for STED fluorescence correlation and time-gated single photon counting. *Bioinformatics.* Epub ahead of print. November 20, 2015; doi:10.1093/bioinformatics/btv687.
36. Sezgin, E., and P. Schwille. 2011. Fluorescence techniques to study lipid dynamics. *Cold Spring Harb. Perspect. Biol.* **3:** a009803.
37. Eggeling, C., C. Ringemann, R. Medda, G. Schwarzmann, K. Sandhoff, S. Polyakova, V. N. Belov, B. Hein, C. von Middendorff, A. Schonle, et al. 2009. Direct observation of the nanoscale dynamics of membrane lipids in a living cell. *Nature.* **457:** 1159–1162.
38. Ringemann, C., B. Harke, C. von Middendorff, R. Medda, A. Honigmann, R. Wagner, M. Leutenegger, A. Schönle, S. Hell, and C. Eggeling. 2009. Exploring single-molecule dynamics with fluorescence nanoscopy. *New J. Phys.* **11:** 103054.
39. Gimpl, G., and K. Gehrig-Burger. 2011. Probes for studying cholesterol binding and cell biology. *Steroids.* **76:** 216–231.
40. Huang, H., A. L. McIntosh, B. P. Atshaves, Y. Ohno-Iwashita, A. B. Kier, and F. Schroeder. 2010. Use of dansyl-cholestanol as a probe of cholesterol behavior in membranes of living cells. *J. Lipid Res.* **51:** 1157–1172.
41. Ohvo-Rekilä, H., B. Akerlund, and J. P. Slotte. 2000. Cyclodextrin-catalyzed extraction of fluorescent sterols from monolayer membranes and small unilamellar vesicles. *Chem. Phys. Lipids.* **105:** 167–178.
42. Honigmann, A., V. Mueller, H. Ta, A. Schoenle, E. Sezgin, S. W. Hell, and C. Eggeling. 2014. Scanning STED-FCS reveals spatiotemporal heterogeneity of lipid interaction in the plasma membrane of living cells. *Nat. Commun.* **5:** 5412.
43. Sheng, R., Y. Chen, H. Yung Gee, E. Stec, H. R. Melowic, N. R. Blatner, M. P. Tun, Y. Kim, M. Kallberg, T. K. Fujiwara, et al. 2012. Cholesterol modulates cell signaling and protein networking by specifically interacting with PDZ domain-containing scaffold proteins. *Nat. Commun.* **3:** 1249.
44. Bagatolli, L. A., S. A. Sanchez, T. Hazlett, and E. Gratton. 2003. Giant vesicles, Laurdan, and two-photon fluorescence microscopy: evidence of lipid lateral separation in bilayers. *Methods Enzymol.* **360:** 481–500.
45. Dietrich, C., L. A. Bagatolli, Z. N. Volovyk, N. L. Thompson, M. Levi, K. Jacobson, and E. Gratton. 2001. Lipid rafts reconstituted in model membranes. *Biophys. J.* **80:** 1417–1428.
46. Sezgin, E., and P. Schwille. 2012. Model membrane platforms to study protein-membrane interactions. *Mol. Membr. Biol.* **29:** 144–154.
47. Klotzsch, E., and G. J. Schuetz. 2013. A critical survey of methods to detect plasma membrane rafts. *Philos. Trans. R. Soc. Lond. B Biol. Sci.* **368:** 20120033.
48. Lozano, M. M., Z. Liu, E. Sunnick, A. Janshoff, K. Kumar, and S. G. Boxer. 2013. Colocalization of the ganglioside G(M1) and cholesterol detected by secondary ion mass spectrometry. *J. Am. Chem. Soc.* **135:** 5620–5630.
49. Frisz, J. F., H. A. Klitzing, K. Lou, I. D. Hutcheon, P. K. Weber, J. Zimmerberg, and M. L. Kraft. 2013. Sphingolipid domains in the plasma membranes of fibroblasts are not enriched with cholesterol. *J. Biol. Chem.* **288:** 16855–16861.
50. Sezgin, E., T. Sadowski, and K. Simons. 2014. Measuring lipid packing of model and cellular membranes with environment sensitive probes. *Langmuir.* **30:** 8160–8166.
51. Sezgin, E., T. Gutmann, T. Buhl, R. Dirkx, M. Grzybek, U. Coskun, M. Solimena, K. Simons, I. Levental, and P. Schwille. 2015. Adaptive lipid packing and bioactivity in membrane domains. *PLoS One.* **10:** e0123930.
52. Baumgart, T., G. Hunt, E. R. Farkas, W. W. Webb, and G. W. Feigenson. 2007. Fluorescence probe partitioning between L-o/L-d phases in lipid membranes. *Biochim. Biophys. Acta.* **1768:** 2182–2194.
53. Kaiser, H. J., D. Lingwood, I. Levental, J. L. Sampaio, L. Kalvodova, L. Rajendran, and K. Simons. 2009. Order of lipid phases in model and plasma membranes. *Proc. Natl. Acad. Sci. USA.* **106:** 16645–16650.
54. Loura, L. M. S., A. Fedorov, and M. Prieto. 2001. Exclusion of a cholesterol analog from the cholesterol-rich phase in model membranes. *Biochim. Biophys. Acta.* **1511:** 236–243.
55. Sevcsik, E., M. Brameshuber, M. Folser, J. Weghuber, A. Honigmann, and G. J. Schutz. 2015. GPI-anchored proteins do not reside in ordered domains in the live cell plasma membrane. *Nat. Commun.* **6:** 6969.
56. Scheidt, H. A., P. Muller, A. Herrmann, and D. Huster. 2003. The potential of fluorescent and spin-labeled steroid analogs to mimic natural cholesterol. *J. Biol. Chem.* **278:** 45563–45569.
57. Kaiser, R. D., and E. London. 1998. Determination of the depth of BODIPY probes in model membranes by parallax analysis of fluorescence quenching. *Biochim. Biophys. Acta.* **1375:** 13–22.
58. Vanier, M. T. 2015. Complex lipid trafficking in Niemann-Pick disease type C. *J. Inherit. Metab. Dis.* **38:** 187–199.
59. Platt, F. M., C. Wassif, A. Colaco, A. Dardis, E. Lloyd-Evans, B. Bembi, and F. D. Porter. 2014. Disorders of cholesterol metabolism and their unanticipated convergent mechanisms of disease. *Annu. Rev. Genomics Hum. Genet.* **15:** 173–194.

60. Peake, K. B., and J. E. Vance. 2010. Defective cholesterol trafficking in Niemann-Pick C-deficient cells. *FEBS Lett.* **584:** 2731–2739.
61. Cruz, J. C., and T. Y. Chang. 2000. Fate of endogenously synthesized cholesterol in Niemann-Pick type C1 cells. *J. Biol. Chem.* **275:** 41309–41316.
62. Pipalia, N. H., M. Hao, S. Mukherjee, and F. R. Maxfield. 2007. Sterol, protein and lipid trafficking in Chinese hamster ovary cells with Niemann-Pick type C1 defect. *Traffic.* **8:** 130–141.
63. Hölttä-Vuori, M., R. L. Uronen, J. Repakova, E. Salonen, I. Vattulainen, P. Panula, Z. G. Li, R. Bittman, and E. Ikonen. 2008. BODIPY-cholesterol: a new tool to visualize sterol trafficking in living cells and organisms. *Traffic.* **9:** 1839–1849.
64. Manson, M. E., D. A. Corey, I. Bederman, J. D. Burgess, and T. J. Kelley. 2012. Regulatory role of beta-arrestin-2 in cholesterol processing in cystic fibrosis epithelial cells. *J. Lipid Res.* **53:** 1268–1276.
65. Du, X., J. Kumar, C. Ferguson, T. A. Schulz, Y. S. Ong, W. Hong, W. A. Prinz, R. G. Parton, A. J. Brown, and H. Yang. 2011. A role for oxysterol-binding protein-related protein 5 in endosomal cholesterol trafficking. *J. Cell Biol.* **192:** 121–135.
66. Lee, H. J., W. Zhang, D. Zhang, Y. Yang, B. Liu, E. L. Barker, K. K. Buhman, L. V. Slipchenko, M. Dai, and J-X. Cheng. 2015. Assessing cholesterol storage in live cells and C. elegans by stimulated Raman scattering imaging of phenyl-diyne cholesterol. *Sci. Rep.* **5:** 7930.
67. Hao, M., S. X. Lin, O. J. Karylowski, D. Wüstner, T. E. McGraw, and F. R. Maxfield. 2002. Vesicular and non-vesicular sterol transport in living cells - The endocytic recycling compartment is a major sterol storage organelle. *J. Biol. Chem.* **277:** 609–617.
68. Wüstner, D., F. W. Lund, C. Röhrl, and H. Stangl. Potential of BODIPY-cholesterol for analysis of cholesterol transport and diffusion in living cells. *Chem. Phys. Lipids.* Epub ahead of print. August 17, 2015; doi:10.1016/j.chemphyslip.2015.08.007.
69. Mondal, M., B. Mesmin, S. Mukherjee, and F. R. Maxfield. 2009. Sterols are mainly in the cytoplasmic leaflet of the plasma membrane and the endocytic recycling compartment in CHO cells. *Mol. Biol. Cell.* **20:** 581–588.
70. Milles, S., T. Meyer, H. A. Scheidt, R. Schwarzer, L. Thomas, M. Marek, L. Szente, R. Bittman, A. Herrmann, T. G. Pomorski, et al. 2013. Organization of fluorescent cholesterol analogs in lipid bilayers - Lessons from cyclodextrin extraction. *Biochim. Biophys. Acta.* **1828:** 1822–1828.
71. Bacia, K., D. Scherfeld, N. Kahya, and P. Schwille. 2004. Fluorescence correlation spectroscopy relates rafts in model and native membranes. *Biophys. J.* **87:** 1034–1043.
72. Mueller, V., C. Ringemann, A. Honigmann, G. Schwarzmann, R. Medda, M. Leutenegger, S. Polyakova, V. N. Belov, S. W. Hell, and C. Eggeling. 2011. STED nanoscopy reveals molecular details of cholesterol- and cytoskeleton-modulated lipid interactions in living cells. *Biophys. J.* **101:** 1651–1660.
73. Vicidomini, G., H. Ta, A. Honigmann, V. Mueller, M. P. Clausen, D. Waithe, S. Galiani, E. Sezgin, A. Diaspro, S. W. Hell, et al. 2015. STED-FLCS: an advanced tool to reveal spatiotemporal heterogeneity of molecular membrane dynamics. *Nano Lett.* **15:** 5912–5918.
74. Magde, D., E. L. Elson, and W. W. Webb. 1974. Fluorescence correlation spectroscopy. II. An experimental realization. *Biopolymers.* **13:** 29–61.
75. Eggeling, C., J. Widengren, R. Rigler, and C. A. Seidel. 1998. Photobleaching of fluorescent dyes under conditions used for single-molecule detection: evidence of two-step photolysis. *Anal. Chem.* **70:** 2651–2659.
76. Solanko, L. M., A. Honigmann, H. S. Midtiby, F. W. Lund, J. R. Brewer, V. Dekaris, R. Bittman, C. Eggeling, and D. Wustner. 2013. Membrane orientation and lateral diffusion of BODIPY-cholesterol as a function of probe structure. *Biophys. J.* **105:** 2082–2092.
77. Hell, S. W., and J. Wichmann. 1994. Breaking the diffraction resolution limit by stimulated emission: stimulated-emission-depletion fluorescence microscopy. *Opt. Lett.* **19:** 780–782.
78. Eggeling, C. 2015. Super-resolution optical microscopy of lipid plasma membrane dynamics. *Essays Biochem.* **57:** 69–80.
79. Eggeling, C., K. I. Willig, S. J. Sahl, and S. W. Hell. 2015. Lens-based fluorescence nanoscopy. *Q. Rev. Biophys.* **48:** 178–243.
80. Maxfield, F. R., and D. Wüstner. 2012. Analysis of cholesterol trafficking with fluorescent probes. *In* Lipids. Vol. 108. G. DiPaolo and M. R. Wenk, editors. 367–393.